Journal of the Serbian Chemical Society
JSCS-info@shd.org.rs • www.shd.org.rs/JSCS

ACCEPTED MANUSCRIPT

Journal of the Serbian Chemical Society
JSCS-info@shd.org.rs • www.shd.org.rs/JSCS
J. Serb. Chem. Soc. **00(0)** 1-25 (2026)
JSCS–13713
Original scientific paper
Published DD MM, 2026

Fabrication of chitosan membrane modified by vanillin and gelatin for crystal violet dye adsorption

KHABIBI KHABIBI*, NABILA AMALIA IZAAZ AANISA AND RETNO ARIADI LUSIANA

Department of Chemistry, Faculty of Sciences and Mathematics, University of Diponegoro 50275 Semarang, Central Java, Indonesia.

(Received 9 January; revised 27 January; accepted 9 April 2026)

Abstract: Crystal violet is a cationic dye that poses serious environmental risks when accumulated in aquatic ecosystems due to its high toxicity to living organisms. Therefore, effective treatment methods are required to remove this dye from wastewater. In this study, a chitosan (Cs)-based bioadsorbent membrane, cross-linked with vanillin (V) and modified with gelatin (G), was developed to adsorb crystal violet dye. The chitosan/vanillin membrane was mixed with gelatin at various concentrations of 0.5% (CsVG1), 0.75% (CsVG2), and 1% (CsVG3). The adsorption process was examined as a function of pH, contact time, initial dye concentration, and temperature. Porosity, swelling degree, water absorption, FTIR, and SEM were included in the membrane's physicochemical characterization. The results showed that the optimal parameters for dye adsorption were pH 6, contact time 80 min, and temperature 298 K, resulting in 88% dye removal. The adsorption kinetics followed a pseudo-second-order model, and the Freundlich model best described the adsorption isotherm. The thermodynamic analysis demonstrated that the adsorption process was spontaneous and exothermic. Thus, the CsVG membrane has the potential to serve as an effective alternative for removing crystal violet from textile industrial wastewater.

Keywords: biopolymers; bioadsorbent; adsorption membrane; dye removal.

INTRODUCTION

Industrial waste containing synthetic dyes poses substantial risks to environmental integrity and public health. Dyes in water can reduce light penetration and lower dissolved oxygen levels, disrupting the photosynthesis of aquatic organisms. Furthermore, these colors have the potential to cause carcinogenic and mutagenic consequences in aquatic creatures and humans.[1] It is estimated that approximately 800,000 tons of dyes are produced each year, of

* Corresponding author. E-mail: khabibi@live.undip.ac.id
https://doi.org/10.2298/JSC260109020K

which about 20% are discharged into water bodies at the final stage of the industrial process.[2] One type of synthetic dye that is widely used is cationic dyes, such as crystal violet. The chemical composition of these dyes is characterized by a complex, highly stable aromatic structure, which renders them difficult to naturally degrade.[3] Crystal violet can significantly reduce the amount of light that passes through and alter the appearance of water, even at low levels.[4] Given these challenges, recent research highlights the importance of developing practical, ecologically friendly ways for removing these dangerous compounds.

Various waste treatment methods have been developed, such as adsorption, flocculation, membrane filtration, photocatalysis and ion exchange.[5,6] Among these technologies, adsorption is a viable approach for dye waste treatment owing to its high efficacy, cost-effectiveness, and operational simplicity. The choice of adsorbent material significantly influences the adsorption process; however, traditional adsorbents, such as commercial activated carbon, have drawbacks including elevated production and regeneration costs, limited selectivity, and reduced reusability.

To improve the efficiency of the adsorption process, bio-based materials are a promising alternative because they are simple, effective, and utilize renewable resources. The increasing demand for environmentally friendly processing technologies has encouraged the use of natural biopolymers as efficient adsorbents. Recent studies show that biopolymers such as cellulose, chitin, and chitosan are gaining attention for dye adsorption applications due to their abundance, affordability, and customizable properties, including surface area, pore size and volume, ease of modification, and environmental sustainability.[7] The review also confirms that chitosan is a superior candidate material as a membrane base for effective dye removal in wastewater treatment.

Chitosan is a biopolymer produced by the deacetylation of chitin extracted from marine crustaceans, formed from basic structural units of amino glucose and N-acetyl amino glucose connected by β-1,4-glycosidic bonds.[8] Chitosan-based adsorbents are effective for dye adsorption owing to their high surface area, numerous functional groups, and good biocompatibility. Chitosan contains numerous amino and hydroxyl groups, crucial for its interaction with dyes.[9,10] Chitosan's solubility in acidic solutions and its limited mechanical strength necessitate physical and chemical changes to improve stability and adsorption efficiency.[11] Vanillin is a phenolic aldehyde that can serve as a natural cross-linking agent due to its non-toxic properties and its ability to enhance the mechanical properties of chitosan membranes, thereby offering a safer alternative to synthetic cross-linking agents such as glutaraldehyde.[11] Gelatin is a mixture of peptides and proteins produced from the controlled hydrolysis of collagen. Gelatin has a high adsorption capacity due to the presence of hydroxyl, carboxyl, and

amino groups along its molecular chain,[12] thereby increasing the number of active sites on the membrane for dye adsorption.

In this study, vanillin-crosslinked chitosan membranes were synthesized via a Schiff base modification reaction on chitosan, then combined with gelatin to increase the number of active sites on the membrane surface during dye removal from aqueous solutions. The chitosan/vanillin/gelatin (CsVG) membrane was characterized to determine its physicochemical properties using swelling degree tests, Fourier Transform Infrared Spectroscopy (FTIR), Scanning Electron Microscopy (SEM), and X-ray Diffraction (XRD). Crystal violet was used as a model toxic cationic dye to assess the adsorption capacity of the CsVG membrane. The adsorption mechanism, isotherm model, kinetics, and thermodynamic parameters were also analyzed to understand the interaction process between the dye and the membrane. The novelty of this research is that there are no reports in the literature showing the use of modified chitosan, vanillin, and gelatin biopolymers as adsorbent membranes for the removal of crystal violet dye. The development of CsVG membranes as adsorbent membranes is expected to be a promising technology for effective, environmentally friendly dye removal from wastewater.

EXPERIMENTAL

Materials

The materials used in this study were chitosan (MW = 40,000 g/mol, DD = 88.5%) (Cv. Bio Chitosan Indonesia), CH_3COOH (MW = 131.11 g/mol) (Merck), NaOH (MW = 40 g/mol) (Merck), Vanillin (MW = 152.15 g/mol) (Merck), Gelatin (Merck), Crystal Violet ($C_{25}H_{30}C_lN_3$)(BM= 407.98 g/mol) (Merck), HCl 37% (Merck) and distilled water.

Synthesis of chitosan membrane

1.5 grams of chitosan is dissolved in 100 mL of 1% acetic acid. The solution is stirred continuously for 24 hours at room temperature. The resulting chitosan solution is poured into a Petri dish and dried at 40-50 °C. The chitosan membrane is immersed in 1 M NaOH, washed with distilled water, and then dried.

Synthesis of chitosan/vanillin/gelatin (CsVG) membrane

Chitosan (1.5 g) was dissolved in 60 mL of 1% acetic acid solution with stirring for 24 hours at room temperature. Separately, vanillin (0.5 g) was dissolved in 100 mL of 1% acetic acid and stirred for 2 hours at 50 °C. The gelatin solution was generated by dissolving gelatin in 100 mL of distilled water at 50 °C with agitation for 2 hours, at concentrations of 0.5% (CsVG1), 0.75% (CsVG2), and 1% (CsVG3) (w/v). The chitosan solution was subsequently combined with 20 mL of vanillin solution and agitated for 4 hours at 60 °C to facilitate cross-linking reactions. Next, the gelatin solution was added to the chitosan-vanillin mixture, and stirring was continued for 24 hours until a homogeneous alloy solution was formed. The resulting solution was then poured into Petri dishes and dried at 50 °C until a membrane was formed. The preparation process of the CsVG membrane is illustrated in Figure 1.

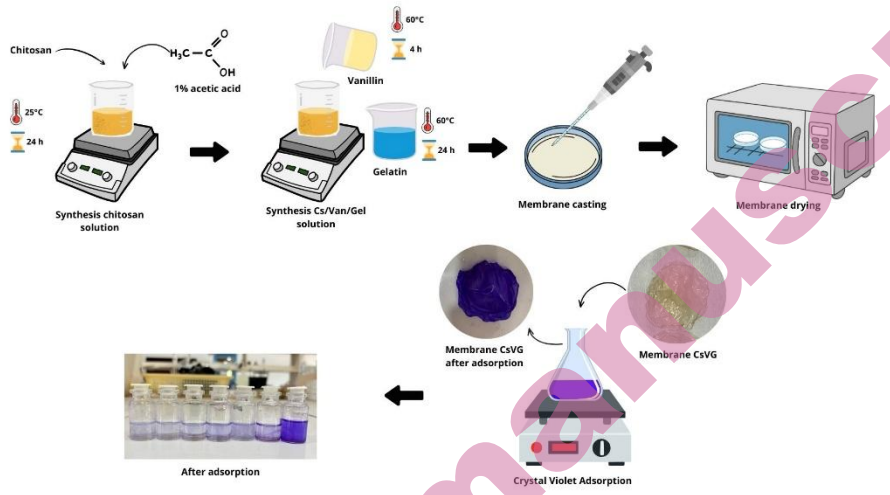

Fig 1. Schematic diagram illustrating the preparation and dye adsorption processes of a Cs/Van/Gel membrane

Characterization of membrane

All CS, CS/Van, and Cs/Van/Gel (CsVG) membranes were characterized using various analytical techniques. Fourier-transform infrared (FTIR) spectra were recorded in the range of 4000–400 cm^{-1} at 1 cm^{-1} resolution with 25 scans per measurement using a Shimadzu FTIR spectrometer to identify changes in functional groups and the formation of new bonds. The crystal structure was analyzed using X-ray diffraction (XRD) using a Rigaku Miniflex 600 instrument with Cu α radiation throughout a 2θ collection range of 3–70° scanning angle with a step size of 0.02° and a scan rate of 1° min. Dye concentrations were analyzed using a UV–Vis spectrophotometer (Shimadzu UV-1280, Serial No. A120660) at the maximum wavelength of each dye. Surface morphology images were obtained using a Scanning Electron Microscope (SEM, Thermo Scientific Quattro S).

pHpzc (pH Point of Zero Charge)

The pHpzc of the membrane was determined through the pH shift method. 50 milliliters of a 0.1M NaCl solution were prepared for the experiment. The pH of the solution was modified to range from 2 to 12 utilizing 0.1 mol NaOH and 0.1 mol HCl. Each solution received 0.05 g of membrane and was allowed to stabilize for 24 hours. The final pH value was recorded. The pHpzc value was determined by plotting ΔpH against pH_i and identifying the point where ΔpH was equal to zero. ΔpH can be calculated by following equation (1)

$$\Delta pH = pH_i - pH_f \quad (1)$$

Where, pH_i is initial pH, pH_f is final pH.[13]

Physical characteristics of membranes

The membrane porosity was determined by the gravimetric method at room temperature and neutral pH. The membrane's initial weight was measured, and it was then immersed in water for 24 hours. The immersed membrane was removed from the water, excess water was removed

by draining on tissue paper, and it was weighed again. For each membrane, the test was repeated three times, and the porosity value was calculated using equation (2)

$$\text{Porosity} = \frac{W_w - W_d}{v \cdot \rho_w} \times 100\% \quad (2)$$

Where W_d is the dry membrane mass (g), W_w is the wet membrane mass after being immersed in distilled water for 24 hours (g), v is the membrane area (cm^3), and ρ_w is the density of water (1 g/cm^3).[14]

To determine the degree of swelling in water, the membrane was measured for its initial and final diameters after immersion in water for 24 hours. The test was conducted three times. The swelling ratio was calculated using equation (3), where l_w is the wet membrane diameter after immersion (cm), and l_d is the dry membrane diameter (cm).[15]

$$\text{Swelling} = \frac{l_w}{l_d} \times 100\% \quad (3)$$

Water absorption was calculated from the dry membrane weight and the membrane weight after 5 hours of soaking. Every hour, the membrane was dried and then weighed. Equation 4 shows the relationship between the wet membrane W_w and the dry membrane W_d to determine the water uptake value.[16]

$$\text{Water uptake} = \frac{W_w - W_d}{W_d} \times 100\% \quad (4)$$

Dye adsorption study

The adsorption test was based on work by Farasati Far.[17] To make a 1000 mg/L stock solution of crystal violet, 1 g of dye was dissolved in 1 L of distilled water until fully dissolved. The initial test was conducted using 50 mL of a 5 mg/L dye solution, with a contact time of 2 hours, a solution temperature of 25°C, and a pH of each experiment set at a minimum value of 4.0 and a maximum value of 8.0 by adding HCl (0.01 M) and NaOH (0.01 M). The dye solution and membrane were placed in an Erlenmeyer flask and stirred with a shaker at 150 rpm. After that, 5 mL of the dye solution was taken, and its absorbance was measured at 591 nm. The test continued with different settings, including contact time (20, 60, 80, 100, and 120 minutes), initial dye concentration (3, 5, 7, 9, and 12 mg/L), and temperature (25, 35, and 45°C). We systematically tested these parameters to determine the optimal conditions for crystal violet adsorption. The dye removal efficiency was determined using equations (5) and (6).

$$q = \frac{(C_i - C_t)}{W} \times V \quad (5)$$

$$Re\% = \frac{(C_i - C_t)}{C_i} \times 100\% \quad (6)$$

Re (%) is the removal efficiency, C_i and C_t (mg/L) are the initial and final concentrations or equilibrium concentrations of the cationic dye crystal violet, V is the solution volume (L), and m is the mass of adsorbent (g).

Adsorption kinetic

The adsorption kinetics of the crystal violet dye were analyzed to understand the rate and mechanism of adsorption. The kinetic study was conducted using two commonly used models: first-order and second-order.

Pseudo-first order kinetics

This analysis is based on the principle that the adsorption rate is directly proportional to the difference between the maximum adsorption capacity and the amount of dye adsorbed at a

given time. Equation 7 and 8 expresses the linear and non-linier form of the pseudo-first-order model.[18]

$$\ln(Q_e - Q_t) = \ln Q_e - k_1 t \quad (7)$$

$$Q_t = Q_e\left(1 - e^{-k_1 t}\right) \quad (8)$$

In this equation, Q_e is the equilibrium adsorption capacity (mg/g), Q_t is the adsorption capacity at time t, k_1 (min^{-1}) is the pseudo first-order rate constant for adsorption, and t is time.

Pseudo-second-order kinetics

The pseudo-second-order kinetic model indicates that the adsorption process is influenced by intricate interactions, such as chemical bonding or the involvement of adsorption sites, suggesting a slow equilibrium system, particularly at elevated concentrations of the substance.[19] The linear and non linier representation of the pseudo-second-order model is delineated in equation 9 and 10.

$$\frac{t}{Q_t} = \frac{1}{k_2 Q_e^2} + \frac{t}{Q_e} \quad (9)$$

$$Q_t = \frac{k_2 Q_e^2 t}{1 + k_2 Q_e t} \quad (10)$$

In this equation, k_2 (g/mg/min) is the rate constant for second-order pseudo adsorption.

Adsorption isotherm

An adsorption isotherm is an absorption phenomenon that occurs at a constant temperature. The adsorption isotherm is studied using the Langmuir and the Freundlich models.

Langmuir isotherm

The Langmuir isotherm model describes adsorption in a single layer (monolayer) on a homogeneous adsorbent surface. This model assumes that the adsorbent surface has a limited number of active sites, each with the same adsorption energy, and that there is no interaction between adsorbed molecules. The linear form of this model is shown in equation 11.[20]

$$\frac{C_e}{Q_e} = \frac{1}{K_L Q_m} + \frac{C_e}{Q_m} \quad (11)$$

Where in this equation C_e is the equilibrium concentration of adsorbate in solution (mg/L), Q_e is the amount of adsorbate adsorbed per unit mass of adsorbent at equilibrium (mg/g), Q_m is the maximum adsorption capacity of the adsorbent (mg/g), and K_L is the Langmuir constant related to the affinity of the adsorbate for the adsorbent (L/mg).

Freundlich isotherm

This model helps calculate heterogeneous adsorption sites on the adsorbent surface. This model allows multilayer adsorption and describes non-ideal, reversible systems. This model is shown in equation 12.

$$\ln Q_e = \ln K_F + \frac{1}{n_F} \ln C_e \quad (12)$$

In this context, Q_e is the amount of dye that has adsorbed at equilibrium (mg/g), and C_e is the concentration of dye in the solution at equilibrium (mg/L). The Freundlich constant, KF, indicates adsorption capacity, and the dimensionless constant n reflects the adsorption intensity. A value of $nF < 1$ suggests favorable conditions for adsorption, whereas a value of $nF > 1$ indicates that adsorption becomes less effective as the concentration increases.[21]

Thermodynamics of adsorption

Optimization of the effect of temperature on dye adsorption was performed to evaluate the thermodynamics of adsorption. Thermodynamic parameters such as Gibbs free energy change (ΔG°), enthalpy change (ΔH°), and entropy change (ΔS°) can be calculated to provide a comprehensive understanding of the adsorption process.[22] Analysis of thermodynamic parameters is useful for analyzing the nature of adsorption interactions and the stability of the complexes formed. The relationship between thermodynamic parameters is presented in equations (13), (14) and (15):[23]

$$G = -RTlnK_c \quad (13)$$

lnK can be calculated using the intercept (ΔS) and slope (ΔH) from the Van't Hoff equation.[24]

$$K_c = \frac{Q_e}{C_e} \times W \quad (14)$$

$$\ln K_c = \frac{\Delta S^\circ}{R} - \frac{\Delta H^\circ}{RT} \quad (15)$$

Q_e is the amount of adsorbate at equilibrium (mg/g), C_e is the concentration of adsorbate at equilibrium (mg/L), W is the weight of adsorbent per volume of solution (g/L), K_c is the adsorption equilibrium constant, R is the gas constant (8.314 J/mol/K), and T is the absolute temperature (K).

RESULTS AND DISCUSSION

Preparation of Cs/Van/Gel (CsVG) membrane

The polymer chain of chitosan, a cationic polysaccharide, has a high density of hydroxyl and amino (-NH_2) groups.[10] A positively charged ammonium group (-NH_3^+) was created by protonating the amino groups (-NH_2) in chitosan after it was dissolved in acetic acid for this investigation. To enhance the membrane's properties, it was modified via vanillin cross-linking. The mechanism of the cross-linking reaction between chitosan and vanillin involves two different stages. The first stage involves the aldehyde group (-CHO) of vanillin reacting with the amine group (-NH_2) of chitosan to form a Schiff base and an imine group (C=N). The imine group (C=N) indicates that chitosan has been successfully cross-linked with vanillin. The covalent bonds formed during cross-linking can increase the membrane's mechanical strength. During the second stage, hydrogen bonds form between the hydroxyl group (-OH) of vanillin and the hydroxyl group (-OH) of chitosan or gelatin, thereby enhancing hydrophilicity and fostering a more organized structure.[25] Gelatin is subsequently incorporated via mixing to enhance the membrane's active areas. The NH_3^+ group on protonated chitosan interacts with the carboxylate (-COO) group on gelatin, which is often negatively charged in solution, thus generating electrostatic interactions.[26] The functional groups on chitosan and gelatin will engage with the target chemicals, establishing hydrogen bonds.

Characterization studies

FTIR Analysis

The FTIR spectrum of the membrane shown in Figure 2 confirms that changes occur at various stages of modification. Based on Figure 2, chitosan shows peaks at 3358 cm^{-1} (O-H stretching) and 3293 cm^{-1} (primary N-H), 2878 cm^{-1} (C-H stretching with CH_2 symmetry), 1644 cm^{-1} and 1589 cm^{-1} (amine twin groups), 1378 cm^{-1} (asymmetric C-H from CH_2) and 1028 cm^{-1} (C-O-C). In the Cs/VAN membrane spectrum, the peaks at 3354 cm^{-1} and 3297 cm^{-1} shifted from the chitosan spectrum due to the formation of hydrogen bonds between the NH_2 of chitosan and the OH of vanillin.[27] The peak at 1644 cm^{-1} in chitosan shifted to 1639 cm^{-1}, indicating C=N stretching vibrations, which showed the formation of a Schiff base bond between the vanillin aldehyde group and the chitosan amine group.[28] The overlap of C=O stretching vibrations originating from the secondary amide group in chitosan can make C=N stretching difficult to identify in the FTIR spectrum.[29] The broad peak at 1588 cm^{-1}, which is the N-H bending group of secondary amine, becomes weaker, indicating that some of the amine groups have been involved in the cross-linking process.[30] In addition, a peak at 1503 cm^{-1} is caused by the benzene ring of vanillin, and a peak at 827 cm^{-1} indicates the bending vibration of the phenolic hydroxyl group in vanillin. This is similar to the study Zhang[31] where the addition of vanillin produced a new peak at a wavelength of 1633 cm^{-1} (C=N), a shift in the absorption peak of the benzene ring from 1584 cm^{-1} to 1586 cm^{-1}, and a peak at 857 cm^{-1} indicating the phenolic –OH group.

In the CsVG1, CsVG2, and CsVG3 membrane spectra, the OH and -NH bands shifted to lower numbers because these peaks indicate intermolecular hydrogen bonds from the hydroxyl group (–OH) and NH stretching from the amide group in gelatin and chitosan. At the same time, the peak at a wavelength of 1637 cm^{-1} confirms the formation of imine bonds (C=N). The C-O and C-N group peaks appear at 1024 cm^{-1}.

XRD Analysis

The XRD patterns of Cs, Cs/VAN, and CsVG2 membranes are shown in Figure 3. Pure Cs exhibits two characteristic semi-crystalline peaks at $2\theta = 10.89°$ and 20.36°,[32] which are related to the partial regularity of the polymer chain due to intra- and intermolecular hydrogen bonds between the $-NH_2$ and $-OH$ groups.[33] The diffraction peak at about 20° (2θ) got wider and less intense after cross-linking with vanillin. It also moved to $2\theta = 22.29°$. This change shows that chitosan and vanillin interact at the molecular level, altering the regularity of the chitosan structure. The lower intensity indicates that crystallinity has decreased because there are fewer free $-NH_2$ groups.[34]

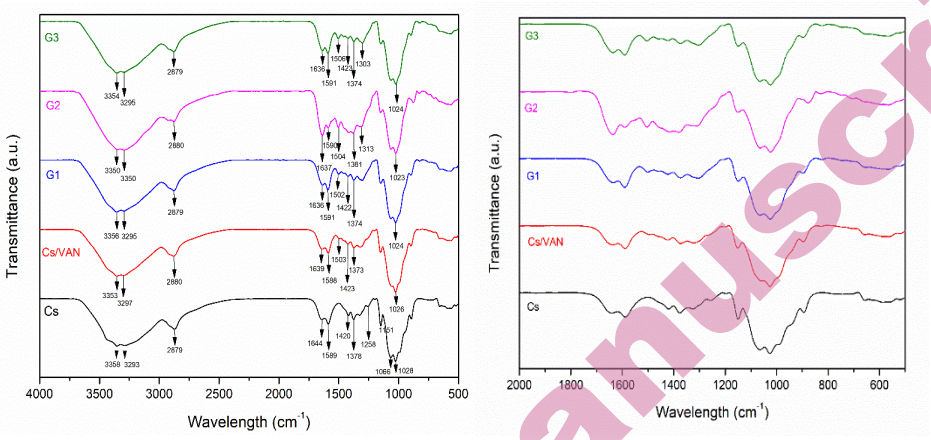

Fig 2. FTIR Spectra of a) Cs, Cs/VAN, G1 (Cs/Van/Gel 0,5%), G2 (Cs/Van/Gel0,75%), G3 (Cs/Van/Gel 1%) and b) FTIR Spectra in 2000-600 cm^{-1}

In the CsVG membrane, a new reflection appears at 2θ = 16.99° and a peak shift from 20.36° and 22.33° (Cs) to 22.42° and 23.39°. The shift to a higher angle indicates a decrease in d-spacing and the formation of a more compact polymer network through interactions among chitosan, vanillin, and gelatin.

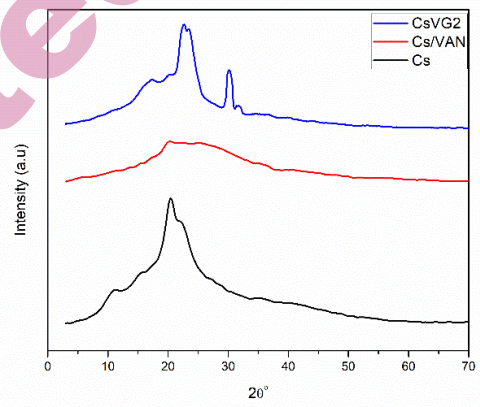

Fig 3. X-ray diffraction of Cs, Cs/VAN, CsVG2

SEM Analysis

Scanning electron microscopy (SEM) analysis images of the Cs, Cs/VAN, and CsVG membrane surfaces are shown in Figure 4.

a. 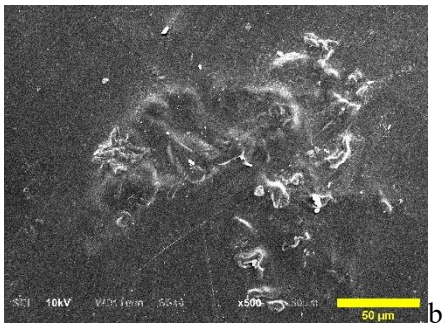

b. 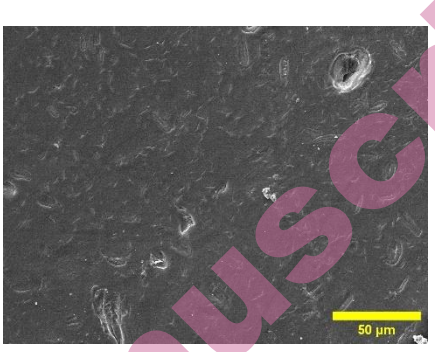

c. 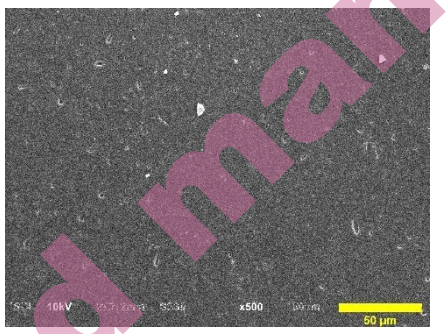

Fig 4. SEM Images at x500 magnification of (a)Cs, (b)Cs/VAN, (c)CsVG2 membrane for adsorption

In Figure 4(a), SEM analysis of the chitosan membrane reveals an uneven, dense surface morphology with no visible voids, indicating reduced permeability and adsorption capacity. Figure 4(b) illustrates the cross-sectional morphology of the Cs/VAN membrane surface, showing a smoother surface accompanied by the formation of cavities. This may be due to cross-linking, which can significantly affect the film's internal microstructure, including cavities, adhesion, smoothness, and compactness. The uniformity of the pores is due to the formation of Schiff bases and hydrogen-bond interactions arising from vanillin cross-links. In Figure 4(c), the CsVG2 membrane with a gelatin concentration of 0.75% exhibits a more consistent, smoother surface than the chitosan and chitosan/vanillin membranes, and it shows visible pores. This indicates the homogeneity between chitosan, gelatin, and vanillin. The addition of gelatin to the membrane produces a smoother surface with a more homogeneous structure, thereby increasing water absorption.[35] Research by Bakouri[36] also shows that cross-sections of arginine-modified chitosan/gelatin films exhibit a similar dense internal structure, indicating a smooth, uniform cross-section. The more porous structure of the CsVG membrane results from electrostatic interactions between chitosan and gelatin, which form a sponge-like structure that enhances the membrane's overall integrity.

pHpzc (pH Point of Zero Charge)

The zero charge point (pHPZC) is the pH value at which the surface charge of the adsorbent is neutral.[13] At pH values below the pHPZC, the adsorbent surface is positively charged, whereas at pH values above the pHPZC, it becomes negatively charged. This surface charge property plays an important role in the adsorption process because it affects the interaction between the adsorbent and the adsorbate. In this study, the cationic dye crystal violet (CV) was used, and it must be adsorbed at a high pH (pH > pHpzc) to achieve maximum adsorption.[37] Based on Figure 5, the pHPZC values obtained were 5.8 for the Cs membrane and 5.6 for the Cs/VAN and CsVG2 membranes.

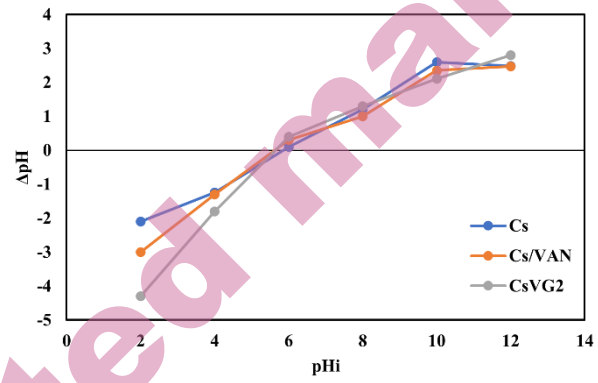

Fig 5. pHpzc graph in the pH range 2-12

Physical characterization of membrane

Porosity, swelling, and water uptake are critical physicochemical parameters in membranes, as they Influence permeation, fouling, and polymer-water interactions, which in turn determine adsorption capacity and kinetics. The results of the physicochemical characterization of the membrane are presented in Figure 6.

To determine the effect of membrane modification with vanillin and gelatin, membrane characteristics, including porosity, degree of swelling, and water absorption, were measured, as shown in Figure 6. Figure 6 shows that porosity, degree of swelling, and water absorption increased linearly. The lowest values were obtained for the pure chitosan membrane, and the physicochemical properties of the membrane increased with increasing modification levels. Among the tested variations, the CsVG2 membrane (Cs/Van/Gel 0.75%) exhibited the best physicochemical characteristics.

Figure 6(a) shows that the porosity of the pure chitosan membrane is 97.99%, whereas in the CsVG2 membrane it increases to 141.86%. This indicates that increasing the gelatin concentration results in a more porous membrane structure.

The presence of carboxyl groups in gelatin increases porosity through electrostatic interactions between chitosan and gelatin.[38] This increase in porosity indicates that the membrane has more empty spaces that can be filled with water, thereby increasing the internal surface area and available pore volume, which ultimately improves adsorption capacity.

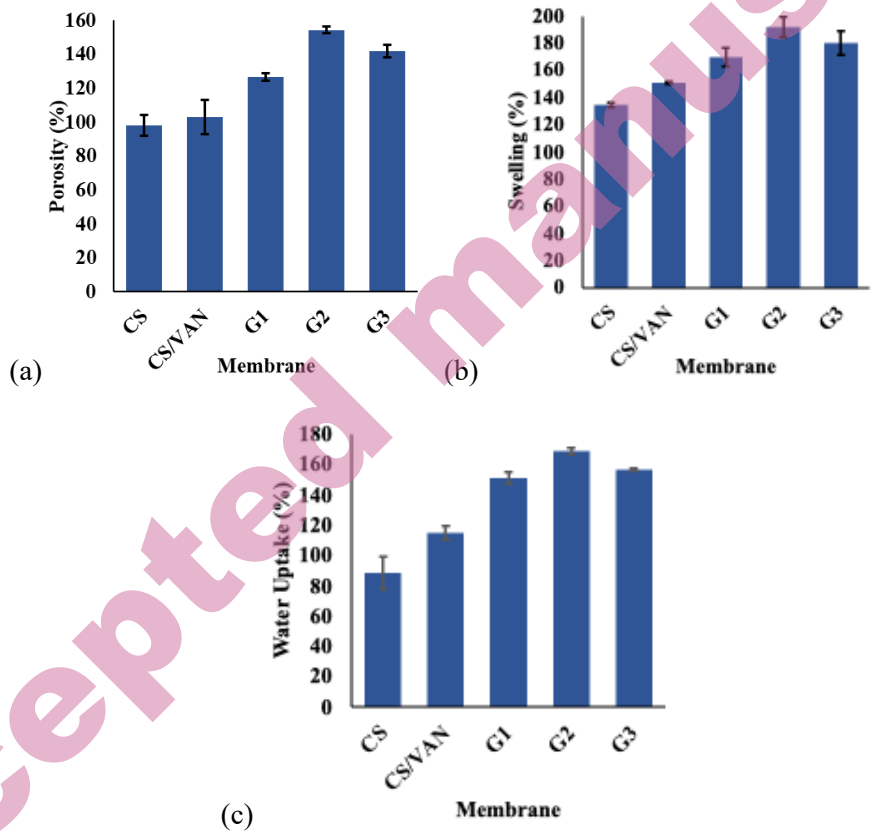

Fig 6. (a) Porosity, (b) swelling, and (c) water uptake for the pure membrane and membrane modification

The degree of swelling values in Figure 6(b) indicates that the lowest swelling occurs in the pure chitosan membrane, at 134.59%. After adding the vanillin cross-linking agent to the Cs/VAN membrane, the degree of swelling increased to 150.60%. The addition of gelatin to the membrane significantly increased the degree of swelling. In the CsVG1 membrane, the swelling value increased to 169.78%, and in the CsVG2 membrane with a gelatin concentration of 0.75%, it reached 191.98%. However, when the gelatin concentration was increased to 1% (CSVG3 membrane), the membrane's expansion decreased to 180.01%. The

formation of cross-links between chitosan and vanillin via the Schiff base reaction produces a more compact membrane structure, reducing the number of available hydrophilic groups and thereby decreasing the membrane's swelling value.[39] However, in this study, the addition of vanillin still increased the degree of expansion. This indicates that the number of remaining hydrophilic groups is still sufficient to allow swelling, in line with the findings reported by Hu.[40]

The increase in the degree of swelling is also supported by the addition of gelatin to the chitosan matrix, because gelatin has carboxyl groups ($–COO^-$) that are hydrophilic and can increase the number of active groups on the membrane surface. A denser polymer network formed by stronger interactions among chitosan, vanillin, and gelatin can reduce swelling at higher gelatin concentrations. This tighter structure makes the membrane less able to absorb and expand with water, as it has less free space and fewer internal pores.

Along with the increase in porosity and degree of expansion, the percentage of water absorption shown in Figure 6(c) indicates that the CsVG2 membrane has the most optimal physicochemical characteristics. A higher water-absorption capacity shows that water molecules are more strongly attracted to the membrane surface, thereby increasing the membrane's hydrophilicity. This increased hydrophilicity is critical to improving membrane performance, as it enhances its ability to absorb dyes.

Adsorption removal of crystal violet

Adsorption with variation in pH

The effect of pH on the adsorption capacity of the Cs/Van/Gel membrane was assessed by adjusting the pH of the dye solution from 4 to 8 at an initial concentration of 5 mg/L. This pH range was chosen because it represents conditions that are practically relevant for dye adsorption applications. Variations in pH are important because solution pH is a significant parameter that affects adsorption, both by altering the adsorbent surface charge and the degree of adsorbate ionization. As shown in Figure 7, the percentage of dye removal increased with increasing solution pH from 4, reached a maximum at pH 6, and then decreased at higher pH values. Under strongly acidic conditions (pH < 4), chitosan may partially dissolve because of excessive protonation of amino groups, leading to structural swelling. Conversely, highly alkaline conditions can result in structural instability.

In acidic environments, the level of H^+ ions is significantly elevated, leading these ions to vie with positively charged Crystal Violet (CV) molecules for negatively charged active sites on the adsorbent's surface. This condition reduces the number of sites available for CV molecules and decreases adsorption efficiency. As pH increases, the number of H^+ decreases, and the adsorbent surface tends to become negatively charged, thereby increasing electrostatic interactions with positively charged CV molecules.[41] However, when the pH is increased from

6 to 7 and 8, CV adsorption decreases. This suggests that, alongside electrostatic forces in the acidic range, mechanisms such as π-π stacking and/or hydrogen bonding are anticipated to become more prominent and potent at neutral or alkaline pH.[42,43]

At pH values above 6, adsorption efficiency decreases again, possibly due to changes in surface charge or the formation of repulsive forces between the adsorbate and adsorbent. Crystal violet is a basic dye with a pKa value of 0.8.[44] With a low pKa, this molecule remains ionized across the experimental pH range, behaving as a cationic dye under all pH conditions tested.

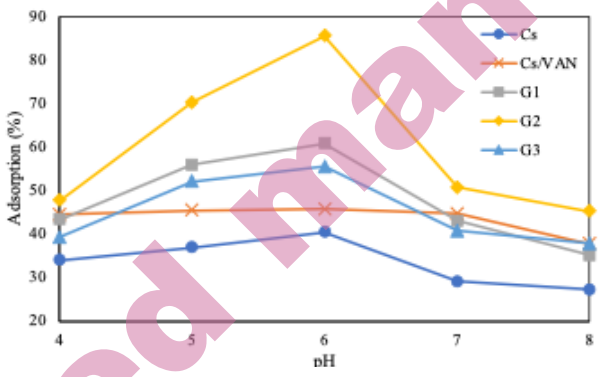

Fig 7. Effect of pH on the CV adsorption efficiency (%) (Initial dye concentration = 5 mg/L, 25 °C, 120 min)

Adsorption with variation in time: kinetic studies

The removal of crystal violet dye by chitosan membranes and modified membranes CsVG is shown in Figure 8. The adsorption capacity of the membrane increased until the 80th minute, which facilitated greater adsorption. Subsequently, the adsorption rate decreased because most active sites were gradually filled, thereby inhibiting the diffusion of crystal violet molecules to the membrane surface. The adsorption capacity of the Cs membrane at 80 minutes was 35.86%, and the maximum adsorption capacity of the CSVG2 membrane reached 85.57%. Based on these data, the optimum adsorption time for crystal violet removal by this membrane system is 80 minutes.

The dye adsorption process was then analyzed using first-order and second-order pseudo-kinetic models. Adsorption kinetics provide information about the adsorption rate, the mechanism of CV adsorption by the membrane, and help determine the possible rate-controlling steps. The experimental data were analyzed using first-order and second-order pseudo-kinetic equations (Equations 6 and 7) via linear and non-linier fitting. Figure 9 illustrates the linearity curves for each model, while the kinetic parameters obtained from this analysis are summarized in Table I.

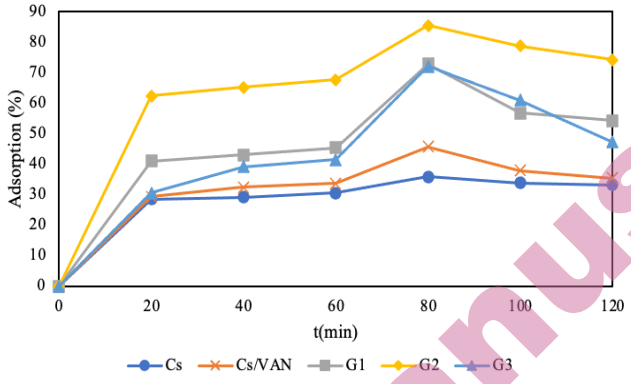

Fig 8. Effect of Contact Time (min) on the CV adsorption efficiency (%) (Initial dye concentration = 5 mg/L; pH = 6).

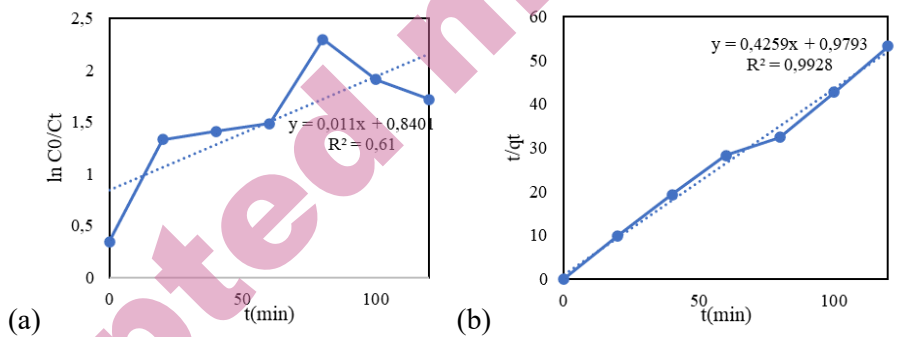

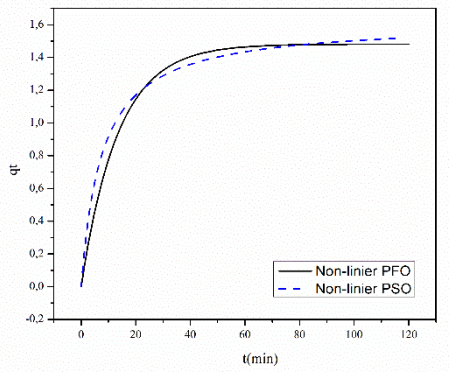

Fig 9. Adsorption Kinetic for (a) Pseudo-first order, (b) Pseudo-second order, (c)non-linier Pseudo-first order and non-linier Pseudo-second order Membrane CsVG

Table I. Adsorption Kinetics Study

Pseudo First Order			
Form	Plot	Parameter	Values
Linier	Ce/qe vs Ce	k_1 (min^{-1})	0,0011
		Qe (mg/g)	2,3165
		R_2	0,61
		SSE	0,8653
Non linier	qt vs t	k_1 (min^{-1})	0,074
		Qe (mg/g)	1,4817
		R_2	0,9549
		SSE	0,0835
Pseudo Second Order			
Form	Plot	Parameter	Values
Linier	log qe vs log Ce	k_2 (g/mg/min)	0,1852
		Qe (mg/g)	2,3479
		R_2	0,9928
		SSE	1,4788
Non linier	qt vs t	k_2 (g/mg/min)	0,0809
		Qe (mg/g)	1,6173
		R_2	0,9648
		SSE	0,065

Based on the kinetic parameters obtained from linear and nonlinear regression analyses, the adsorption process is better described by the pseudo-second-order (PSO) model than by the pseudo-first-order (PFO) model. The PSO model yielded higher determination coefficients (R^2 = 0.9928 and 0.9648) than the PFO model. Due to potential changes in the error structure from linearization, model suitability was primarily assessed using nonlinear regression and SSE values. The PSO model demonstrated a lower SSE, signifying a better fit to the experimental data. The fit of the PSO model with the experimental data showed that the adsorption rate was controlled by the interaction between the active sites of the adsorbent and the dye molecules, where the dye binding process involved the exchange or sharing of electron pairs between the active sites of the adsorbent and the cationic groups on the adsorbate.[45] Other studies by Agbor Tabi[46] and Ahmad and Ejaz[47] also show that the crystal violet dye is adsorbed via chemisorption.

Adsorption with variation in initial concentration of adsorbates

The effect of initial dye concentration on adsorption was studied by varying the concentration of crystal violet in the range of 3, 5, 7, 9, and 12 mg/L. Conversely, other adsorption variables were kept constant, namely pH = 6.0 and adsorption time of 80 minutes.

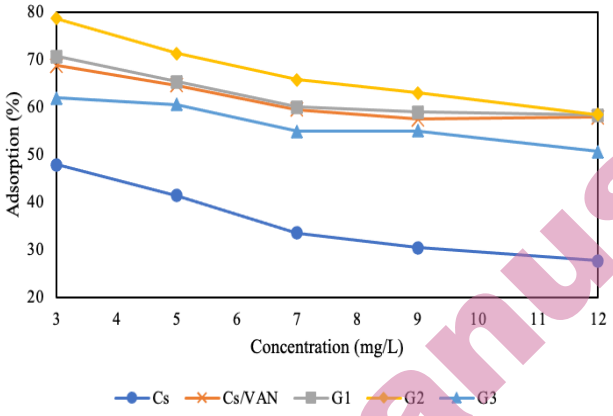

Fig 10. Effect of Dye Concentration (mg/L) on the CV adsorption efficiency (%) (pH=6,0; t= 80 min)

Based on the results shown in Figure 10, increasing the initial dye concentration gradually decreases the adsorption efficiency. At low crystal violet concentrations, the number of dye molecules is relatively proportional to the number of active sites available on the membrane surface, so that CV molecules can be easily adsorbed through various interaction mechanisms, such as hydrogen bonding, electrostatic interactions, and π–π interactions between the CsVG membrane and the functional groups of crystal violet. At higher crystal violet concentrations, the number of dye molecules increases, but the number of available active sites remains limited. This discrepancy between the number of dye molecules and the number of available adsorption sites reduces the effectiveness of adsorption.[48]

The adsorption performance of crystal violet on CsVG membranes was evaluated using adsorption isotherm studies with the Langmuir and the Freundlich models. The results of the isotherm studies were used to determine the qualitative properties of the adsorbate-adsorbent systems. According to the Langmuir adsorption isotherm, adsorption occurs in a monolayer on a homogeneous surface. In contrast, the Freundlich isotherm refers to the amount of adsorbate absorbed per unit mass of adsorbent in a heterogeneous system. The results of the CsVG membrane isotherm study are shown in Figure 11 and Table II.

The adsorption process can be determined by the highest regression coefficient value (R^2) based on the isotherm parameters and membrane regression coefficients in Table II. The R^2 value for the Cs membrane in Langmuir is 0.9693 and in Freundlich is 0.9873, while in the CsVG2 membrane (Cs/Van/Gel 0.75%), the R^2 value in Langmuir is 0.9657 and in Freundlich is 0.9989. This finding suggests that the crystal violet adsorption system on all adsorbents follows the Freundlich isotherm model, as evidenced by an R^2 value exceeding the Langmuir

model threshold and approaching 1. The Freundlich isotherm model assumes adsorption on a heterogeneous surface, leading to the formation of a multilayer. Additionally, the phenomenon is attributed to physical adsorption via van der Waals or weak interactions between crystal violet and the adsorbent surface.[49]

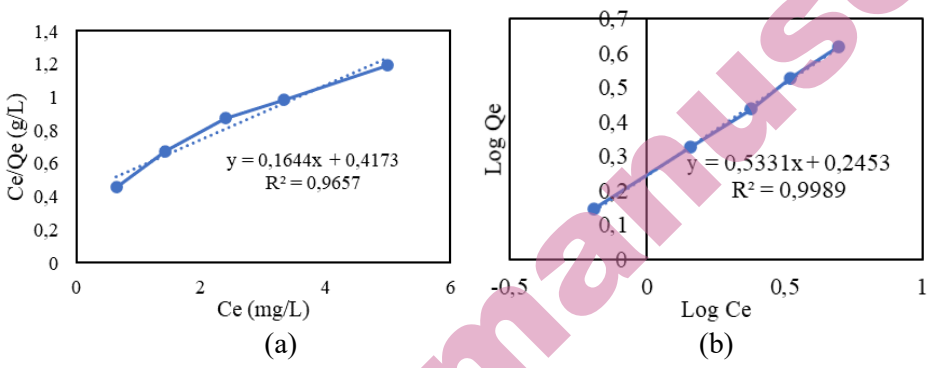

Fig 11. (a) Langmuir and (b) Freundlich adsorption isotherm studies for CsVG membrane

Table II. Isotherm Adsorption Study

Membrane	Langmuir			Freundlich		
	K_L (L/mg)	Qmax (mg/g)	R^2	Kf (L/mg)	n	R^2
Cs	2,6205	0,2683	0,9693	0,7796	2,1372	0,9873
Cs/VAN	8,5034	0,1633	0,8456	0,9880	1,4438	0,9896
CsVG1	8,1766	0,1823	0,854	0,8958	1,4925	0,99
CsVG2	6,0827	0,3939	0,9657	0,6103	1,8758	0,9989
CsVG3	7,8247	0,1440	0,9528	1,0899	1,3976	0,99

Adsorption with variation in temperature: thermodynamic studies

The effect of temperature on the adsorption process is shown in Figure 12. The temperature variations used in this experiment were 298, 308, 318, and 328 K. The best results were obtained with the CsVG2 membrane (Cs/Van/Gel 0.75%), which achieved adsorption percentages of 88.12% at 298 K and 47.33% at 328 K. The adsorption efficiency of crystal violet decreased with increasing temperature.

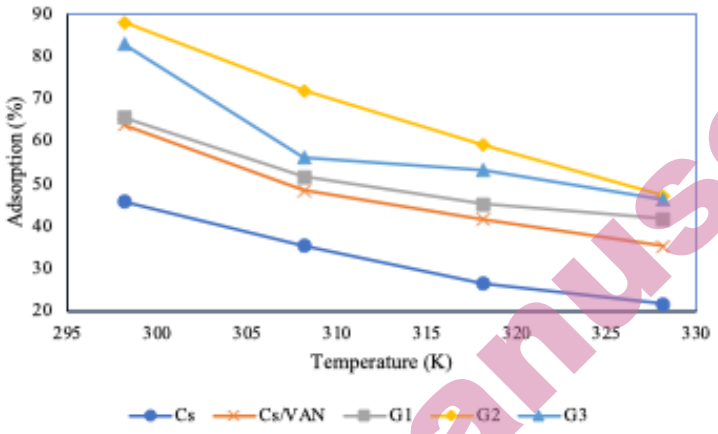

Fig 12. Effect of Temperature (K) on the CV adsorption efficiency (%) (pH=6,0; t= 80 min: dye concentration= 3 mg/L)

The exothermic nature of the adsorption process is indicated by a decrease in adsorption capacity with increasing temperature. Thermodynamic parameters used to describe the adsorption process, such as standard free energy (G°), enthalpy change (H°), and entropy change (S°), support this occurrence. As shown in Figure 13, the slope and intercept of the van't Hoff plot of lnKc vs 1/T are used to obtain the values of △H and △S. Table III presents the results of the thermodynamic parameter calculations.

According to Table III, as the temperature increases, the ΔG° value indicates that the adsorption process becomes more spontaneous. The negative ΔH° value indicates that the adsorption process for crystal violet is exothermic. The ΔS° value yields good affinity between the CsVG2 membrane and crystal violet, thereby reducing unpredictability at the solid/liquid interface during adsorption.

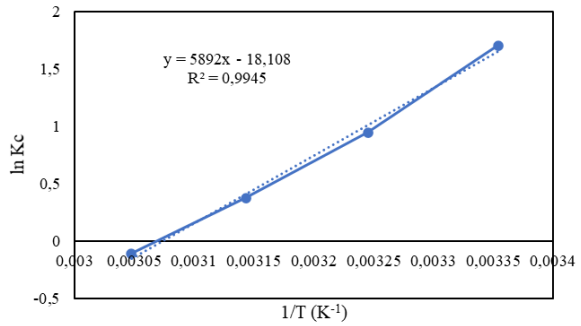

Fig 13. Thermodynamics for the adsorption of CV dye onto CsVG Membrane (Time = 80 min; dye concentration = 3 mg/L; pH = 6)

Table III. Thermodynamic parameters for CV

Membrane	Temperature (K)	ΔG° (J/mol)	ΔH° (kJ/mol)	ΔS° (J/mol.K)
Cs	298,15	-201	-32,86	-111
	308,15	-1489		
	318,15	-2684		
	328,15	-3490		
CsVG2	298,15	-4229	-48,98	-150
	308,15	-2429		
	318,15	-1001		
	328,15	-291		

Interactions between CsVG membrane and the adsorbates

The adsorption mechanism depends on the functional groups and surface porosity of the adsorbent and adsorbate molecules. An estimate of the mechanism by which the membrane-bound active groups interact with crystal violet is shown in Figure 14.

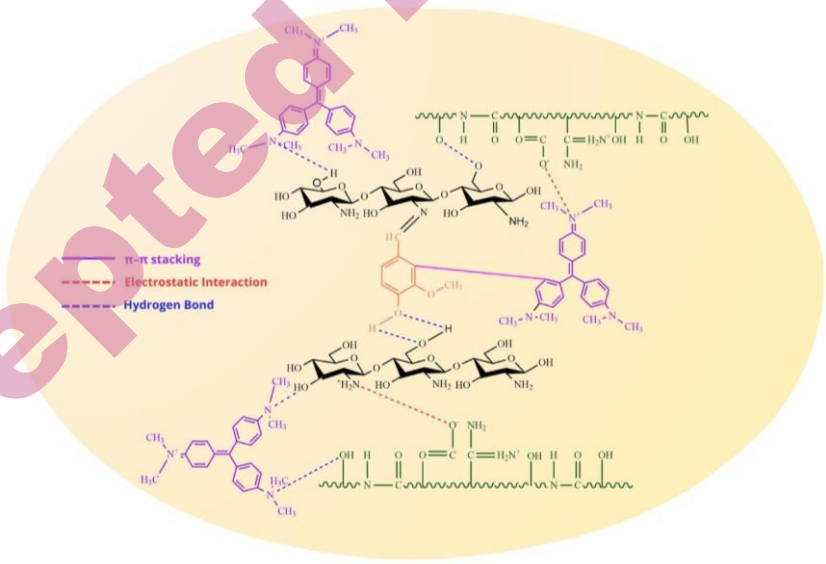

Fig 14. Estimated adsorption mechanism

Possible reaction mechanisms between the active sites on the surface of the chitosan/vanillin/gelatin membrane and crystal violet include electrostatic interactions, π-π interactions, and hydrogen bonding. Electrostatic bonds occur between the negative charge of the $–COO^-$ group in gelatin and the positive group (N^+) in crystal violet. The hexagonal structure of vanillin and the benzene ring of crystal violet can enhance adsorption by acting as electron donors and acceptors

via π-π stacking. In addition, H atoms from functional groups containing O on the surface of the CsVG membrane can form hydrogen bonds with N atoms in crystal violet.

Reusability study

Reusability and stability are important parameters in evaluating the performance of adsorbents for water treatment. Therefore, the Cs and CsVG2 membranes were retested at the optimum pH during three consecutive adsorption cycles. Based on Figure 15, initial use showed the highest adsorption efficiency. After three cycles, the CsVG2 membrane still maintained a fairly high adsorption capacity, although the efficiency of crystal violet (CV) adsorption decreased from 89% to 49%. This reduction in efficiency is probably caused by some CV molecules being strongly bound to active sites via electrostatic interactions, π–π interactions, or hydrogen bonds. As a result, the number of available active sites is reduced. In addition, pore blocking by residual dye molecules may occur, inhibiting the diffusion of adsorbates into the membrane structure. This decrease indicates that optimization of the regeneration method is still needed to improve membrane reuse performance.

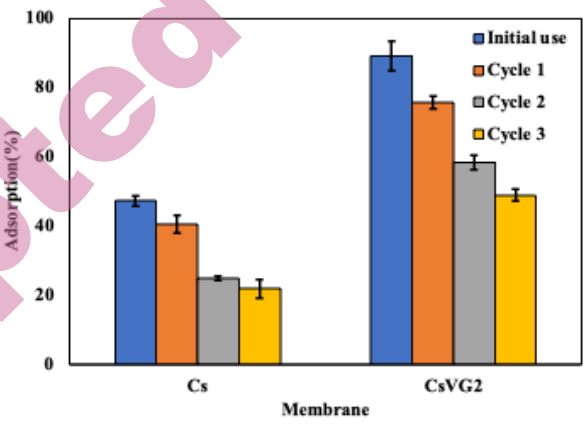

Fig 15. The cycles of reusability membrane (%)

CONCLUSION

In this study, CsVG membranes were developed from chitosan crosslinked with vanillin and modified with varying concentrations of gelatin (0.5%; 0.75%; and 1%). The modified membranes exhibited good adsorption of crystal violet, with the optimum membrane (CSVG2) obtained at a gelatin concentration of 0.75%. The addition of vanillin and gelatin improved the physical characteristics of the membrane, such as porosity, swelling, and water absorption, in comparison to the pure chitosan membrane. The optimal parameters for dye adsorption were

identified as pH 6, a contact time of 80 minutes, an initial dye concentration of 3 mg/L, and a temperature of 298 K, yielding 88% dye removal.

The kinetics of adsorption conformed to a pseudo-second-order model, suggesting that both the duration and the concentration of the dye influenced the rate of adsorption and that chemical interactions took place between the adsorbent and the adsorbate. The isotherm best fits the Freundlich model, with an R2 value of 0.9989 at 298 K. The thermodynamic results show that the adsorption process is exothermic ($\Delta H° < 0$) and spontaneous ($\Delta G° < 0$).

Overall, the results of this study indicate that the CsVG bioadsorbent membrane has good physicochemical properties and the potential to be developed as an effective, environmentally friendly adsorbent for the removal of crystal violet dye from liquid waste. Further research is needed to evaluate the membrane's regeneration and reuse capabilities and to examine its application in more complex wastewater systems.

Acknowledgements: The authors would like to acknowledge the Institute for Research and Community Service, Diponegoro University, for its support through the 2025 research program.

И З В О Д

ИЗРАДА ХИТОЗАНСКЕ МЕМБРАНЕ МОДИФИКОВАНЕ ВАНИЛИНОМ И ЖЕЛАТИНОМ ЗА АДСОРПЦИЈУ КРИСТАЛНО ЉУБИЧАСТЕ БОЈЕ

KHABIBI KHABIBI*, NABILA AMALIA IZAAZ AANISA, RETNO ARIADI LUSIANA

Department of Chemistry, Faculty of Sciences and Mathematics, University of Diponegoro 50275 Semarang, Central Java, Indonesia .

Кристално љубичаста је катјонска боја која представља озбиљне ризике по животну средину када се акумулира у воденим екосистемима због своје високе токсичности за живе организме. Због тога су потребне ефикасне методе третмана за уклањање ове боје из отпадних вода. У овој студији, хитозанска (Cs) биоадсорбент мембрана, умрежена са ванилином (V) и модификована желатином (G), је развијена за апсорпцију кристално љубичасте боје. Хитозан / ванилин мембрана је помешана са желатином у различитим концентрацијама 0.5% (CsVG1), 0.75% (CsVG2), и 1% (CsVG3). Процес адсорпције је испитан у функцији pH, времена контакта, почетне концентрације боје и температуре. Мембрана је окарактерисана мерењем порозности , степеном бубрења, апсорпцијом воде, FTIR, и SEM. Резултати су показали да су оптимални параметри за адсорпцију боје били pH 6, време контакта 80 мин и температура 298 K, што је резултирало уклањањем 88% боје. Кинетика адсорпције пратила је модел псеудо-другог реда, а Freundlich модел најбоље је описао изотерму адсорпције. Термодинамичка анализа је показала да је процес адсорпције био спонтан и егзотерман. Дакле , CsVG мембрана има потенцијал да послужи као ефикасна алтернатива за уклањање кристално љубичасте из текстилних индустријских отпадних вода.

(Примљено 9. јануара; ревидирано 27. јануара; прихваћено 9. априла 2026.)

REFERENCES

1. E. Alver, A. Ü. Metin, *Chem. Eng. J.* **200–202** (2012) 59–67 (https://doi.org/10.1016/j.cej.2012.06.038)
2. M. Greluk, Z. Hubicki, *Desalination* **278** (2011) 219–226 (https://doi.org/10.1016/j.desal.2011.05.024)
3. C. Ruiz, M. Vera, B. L. Rivas, S. Sánchez, B. F. Urbano, *RSC Adv.* **10** (2020) 43799–43810 (https://doi.org/10.1039/D0RA08188D)
4. A. K. Hady, M. E. Owda, R. E. Abouzeid, H. A. Shehata, A. S. Elzaref, A. S. Elfeky, *Biomass Convers. Biorefinery* **15** (2025) 759–773 (https://doi.org/10.1007/s13399-023-05146-0)
5. R. Mohammad-Rezaei, B. Khalilzadeh, F. Rahimi, S. Moradi, M. Shahlaei, H. Derakhshankhah, M. Jaymand, *Environ. Res.* **214** (2022) 113966 (https://doi.org/10.1016/j.envres.2022.113966)
6. D. Ordonez, A. Valencia, B. Pereira, N.-B. Chang, *Environ. Res.* **212** (2022) 113208 (https://doi.org/10.1016/j.envres.2022.113208)
7. R. S. Dassanayake, S. Acharya, N. Abidi, *Molecules* **26** (2021) 4697 (https://doi.org/10.3390/molecules26154697)
8. X. Zhao, X. Wang, T. Lou, *J. Hazard. Mater.* **403** (2021) 124054 (https://doi.org/10.1016/j.jhazmat.2020.124054)
9. W. Liu, T. Lou, X. Wang, *Int. J. Biol. Macromol.* **242** (2023) 124711 (https://doi.org/10.1016/j.ijbiomac.2023.124711)
10. C. Miao, W. Huang, K. Li, Y. Yang, *Environ. Res.* **263** (2024) 120195 (https://doi.org/10.1016/j.envres.2024.120195)
11. B. Tomadoni, A. Ponce, M. Pereda, M. R. Ansorena, *Polym. Test.* **78** (2019) 105935 (https://doi.org/10.1016/j.polymertesting.2019.105935)
12. R. Resmi, S. Unnikrishnan, L. K. Krishnan, V. Kalliyana Krishnan, *J. Appl. Polym. Sci.* **134** (2017) (https://doi.org/10.1002/app.44529)
13. D. Mangla, A. Sharma, S. Ikram, *React. Funct. Polym.* **175** (2022) 105261 (https://doi.org/10.1016/j.reactfunctpolym.2022.105261)
14. R. A. Lusiana, N. B. A. Prasetya, K. Khabibi, *Indones. J. Chem. Sci.* **9** (2020) 194–200 (https://journal.unnes.ac.id/sju/ijcs/article/view/41759/17209) (*In Indonesian*)
15. J. Yuan, Z.-Z. Pan, Y. Jin, Q. Qiu, C. Zhang, Y. Zhao, Y. Li, *J. Power Sources* **500** (2021) 229983 (https://doi.org/10.1016/j.jpowsour.2021.229983)
16. U. S. Malik, Q. Duan, M. B. K. Niazi, Z. Jahan, U. Liaqat, F. Sher, Y. Gan, H. Hou, *Chinese Chem. Lett.* **34** (2023) 108071 (https://doi.org/10.1016/j.cclet.2022.108071)
17. B. Farasati Far, M. R. Naimi-Jamal, M. Jahanbakhshi, S. A. Khalafvandi, M. Alian, D. Razeghi Jahromi, *J. Mol. Liq.* **395** (2024) 123839 (https://doi.org/10.1016/j.molliq.2023.123839)
18. N. Parshi, D. Pan, V. Dhavle, B. Jana, S. Maity, J. Ganguly, *Int. J. Biol. Macromol.* **141** (2019) 626–635 (https://doi.org/10.1016/j.ijbiomac.2019.09.025)
19. C. Ye, B. Yan, X. Ji, B. Liao, R. Gong, X. Pei, G. Liu, *Ecotoxicol. Environ. Saf.* **180** (2019) 366–373 (https://doi.org/10.1016/j.ecoenv.2019.04.086)
20. S. El Bourachdi, A. El Amri, A. R. Ayub, F. Moussaoui, Y. Rakcho, F. El Ouadrhiri, A. Adachi, M. Lechheb, J. A. Herrera-Melián, A. Lahkimi, *Int. J. Biol. Macromol.* **305** (2025) 141030 (https://doi.org/10.1016/j.ijbiomac.2025.141030)
21. G. Purwiandono, P. Lestari, *J. Ecol. Eng.* **24** (2023) 137–145 (https://doi.org/10.12911/22998993/166319)

22. L.-C. Juang, C.-C. Wang, C.-K. Lee, *Chemosphere* **64** (2006) 1920–1928 (https://doi.org/10.1016/j.chemosphere.2006.01.024)
23. S. Jabbarvand Behrouz, A. Khataee, M. Safarpour, S. Arefi-Oskoui, S. Woo Joo, *Sep. Purif. Technol.* **269** (2021) 118720 (https://doi.org/10.1016/j.seppur.2021.118720)
24. S. Wang, H. Wang, S. Wang, L. Fu, L. Zhang, *Sep. Purif. Technol.* **307** (2023) 122783 (https://doi.org/10.1016/j.seppur.2022.122783)
25. H. Yu, Y. Ge, H. Ding, Y. Yan, L. Wang, *Int. J. Biol. Macromol.* **253** (2023) 126726 (https://doi.org/10.1016/j.ijbiomac.2023.126726)
26. S. J. Peighambardoust, S. Imani Zardkhaneh, M. Foroughi, R. Foroutan, H. Azimi, B. Ramavandi, *Environ. Res.* **258** (2024) 119428 (https://doi.org/10.1016/j.envres.2024.119428)
27. G. Michailidou, E. N. Koukaras, D. N. Bikiaris, *Int. J. Biol. Macromol.* **192** (2021) 1266–1275 (https://doi.org/10.1016/j.ijbiomac.2021.10.093)
28. C. Xu, W. Zhan, X. Tang, F. Mo, L. Fu, B. Lin, *Polym. Test.* **66** (2018) 155–163 (https://doi.org/10.1016/j.polymertesting.2018.01.016)
29. R. L. C. G. da Silva, O. D. Bernardinelli, E. C. G. Frachini, H. Ulrich, E. Sabadini, D. F. S. Petri, *Carbohydr. Polym.* **292** (2022) 119725 (https://doi.org/10.1016/j.carbpol.2022.119725)
30. J. R. Westlake, M. Laabei, Y. Jiang, W. C. Yew, D. L. Smith, A. D. Burrows, M. Xie, *ACS Food Sci. Technol.* **3** (2023) 1680–1693 (https://doi.org/10.1021/acsfoodscitech.3c00222)
31. Z. Zhang, J. Zhao, W. Li, H. Yuan, Y. Chi, J. Tang, J. Wang, Z. Xie, *J. Environ. Chem. Eng.* **13** (2025) 118743 (https://doi.org/10.1016/j.jece.2025.118743)
32. M. Carpintero, I. Marcet, C. Cortizo, P. Guerrero, K. de la Caba, M. Rendueles, M. Díaz, *Food Hydrocoll.* **171** (2026) 111838 (https://doi.org/10.1016/j.foodhyd.2025.111838)
33. Y. Peng, Y. Yu, Z. Su, Y. Zhong, S. Vijayakumar, Y. Chen, Y. Mao, M. Xin, M. Li, *Carbohydr. Polym.* **367** (2025) 124015 (https://doi.org/10.1016/j.carbpol.2025.124015)
34. Y. Yang, Y. Zhang, G. Wang, Z. Yang, J. Xian, Y. Yang, T. Li, Y. Pu, Y. Jia, Y. Li, Z. Cheng, S. Zhang, X. Xu, *J. Environ. Chem. Eng.* **9** (2021) 105407 (https://doi.org/10.1016/j.jece.2021.105407)
35. L. Chen, H.-H. Cheng, J. Xiong, Y.-T. Zhu, H.-P. Zhang, X. Xiong, Y.-M. Liu, J. Yu, Z.-X. Guo, *Chinese J. Polym. Sci.* **36** (2018) 1063–1069 (https://doi.org/10.1007/s10118-018-2112-0)
36. H. Bakouri, A. Ziane, K. Guemra, *Int. J. Biol. Macromol.* **230** (2023) 123181 (https://doi.org/10.1016/j.ijbiomac.2023.123181)
37. F. Mashkoor, A. Nasar, C. Jeong, *Biomass Convers. Biorefinery* **14** (2024) 313–325 (https://doi.org/10.1007/s13399-021-02282-3)
38. S. Haider, S. Y. Park, S. H. Lee, *Soft Matter* **4** (2008) 485–492 (https://doi.org/10.1039/b713944f)
39. S. Amjadi, S. Emaminia, S. Heyat Davudian, S. Pourmohammad, H. Hamishehkar, L. Roufegarinejad, *Carbohydr. Polym.* **216** (2019) 376–384 (https://doi.org/10.1016/j.carbpol.2019.03.062)
40. J. Hu, Z. Wang, J. M. Miszuk, M. Zhu, T. I. Lansakara, A. V. Tivanski, J. A. Banas, H. Sun, *Carbohydr. Polym.* **271** (2021) 118440 (https://doi.org/10.1016/j.carbpol.2021.118440)

41. H. Mittal, A. Al Alili, P. P. Morajkar, S. M. Alhassan, *J. Mol. Liq.* **323** (2021) 115034 (https://doi.org/10.1016/j.molliq.2020.115034)
42. S. A. Ganiyu, M. A. Suleiman, W. A. Al-Amrani, A. K. Usman, S. A. Onaizi, *Sep. Purif. Technol.* **318** (2023) 123765 (https://doi.org/10.1016/j.seppur.2023.123765)
43. S. A. Bahadi, M. Iddrisu, M. K. Al-Sakkaf, M. A. A. Elgzoly, Q. A. Drmosh, W. A. Al-Amrani, U. Ahmed, U. Zahid, S. A. Onaizi, *Emergent Mater.* **7** (2024) 959–971 (https://doi.org/10.1007/s42247-023-00513-z)
44. H. Jayasantha Kumari, P. Krishnamoorthy, T. K. Arumugam, S. Radhakrishnan, D. Vasudevan, *Int. J. Biol. Macromol.* **96** (2017) 324–333 (https://doi.org/10.1016/j.ijbiomac.2016.11.077)
45. C. Zhou, S. Lee, K. Dooley, Q. Wu, *J. Hazard. Mater.* **263** (2013) 334–341 (https://doi.org/10.1016/j.jhazmat.2013.07.047)
46. G. Agbor Tabi, L. Ngouateu Rene Blaise, K. Daouda, A. Naphtali Odogu, A. Aime Victoire, N. Nsami Julius, K. Joseph Mbadcam, *Arab. J. Chem.* **15** (2022) 103515 (https://doi.org/10.1016/j.arabjc.2021.103515)
47. R. Ahmad, M. O. Ejaz, *Dye. Pigment.* **216** (2023) 111305 (https://doi.org/10.1016/j.dyepig.2023.111305)
48. A. Salah Omer, G. A.El Naeem, A. I. Abd-Elhamid, O. O.M. Farahat, A. A. El-Bardan, H. M.A. Soliman, A. A. Nayl, *J. Mater. Res. Technol.* **19** (2022) 3241–3254 (https://doi.org/10.1016/j.jmrt.2022.06.045)
49. L. Liu, Z. Y. Gao, X. P. Su, X. Chen, L. Jiang, J. M. Yao, *ACS Sustain. Chem. Eng.* **3** (2015) 432–442 (https://doi.org/10.1021/sc500848m).